



Self-assembled three-dimensional macroscopic graphene/MXene-based hydrogel as electrode for supercapacitor

Cite as: APL Mater. **8**, 091101 (2020); <https://doi.org/10.1063/5.0015426>

Submitted: 27 May 2020 . Accepted: 12 August 2020 . Published Online: 09 September 2020

 Luojiang Zhang, and  Siu Wing Or



View Online



Export Citation



CrossMark

ARTICLES YOU MAY BE INTERESTED IN

Recent advancements in the study of intrinsic magnetic topological insulators and magnetic Weyl semimetals

APL Materials **8**, 090701 (2020); <https://doi.org/10.1063/5.0015328>

Electrochemical impedance spectroscopy of human cochleas for modeling cochlear implant electrical stimulus spread

APL Materials **8**, 091102 (2020); <https://doi.org/10.1063/5.0012514>

Conductive coatings of 2D MXene-in water for electronics applications

AIP Conference Proceedings **2263**, 050003 (2020); <https://doi.org/10.1063/5.0017436>

 Measure Ready
FastHall™ Station

The highest performance tabletop system
for van der Pauw and Hall bar samples



Learn more

 Lake Shore
CRYOTRONICS



Self-assembled three-dimensional macroscopic graphene/MXene-based hydrogel as electrode for supercapacitor

Cite as: APL Mater. 8, 091101 (2020); doi: 10.1063/5.0015426

Submitted: 27 May 2020 • Accepted: 12 August 2020 •

Published Online: 9 September 2020



View Online



Export Citation



CrossMark

Luojiang Zhang^{1,2}  and Siu Wing Or^{1,2,a)} 

AFFILIATIONS

¹Department of Electrical Engineering, The Hong Kong Polytechnic University, Hung Hom, Kowloon, Hong Kong

²Hong Kong Branch of National Rail Transit Electrification and Automation Engineering Technology Research Center, Kowloon, Hong Kong

^{a)}Author to whom correspondence should be addressed: eeswor@polyu.edu.hk

ABSTRACT

Hydrogels with unique three-dimensional (3D) macroscopic porous architectures are attractive electrode materials for supercapacitors because of their superior electrolyte permeabilities and rapid electron/ion transports. In this letter, a cylindrical-type 3D macroscopic graphene/MXene-based hydrogel (GMH) is prepared by self-assembling laminar-structured graphene oxide (GO) and MXene (Ti_3C_2) nanosheets via a facile one-step hydrothermal method under the existence of ammonia water and hydrazine hydrate. GO is found to self-converge into a 3D macroscopic porous graphene framework during the hydrothermal process, while Ti_3C_2 nanosheets are able to prevent the graphene nanosheets from self-restacking. The as-prepared GMH shows a larger specific surface area of $161.1 \text{ m}^2 \text{ g}^{-1}$ and a higher pore volume of $0.5 \text{ cm}^3 \text{ g}^{-1}$ in comparison with the pure graphene hydrogel. A symmetric supercapacitor utilizing GMH as electrodes exhibits high energy densities of 9.3 Wh kg^{-1} and 5.7 Wh kg^{-1} at different power densities of 500 W kg^{-1} and 5000 W kg^{-1} , respectively, as well as an outstanding long-term cycle stability with no loss in capacitance in excess of 10 000 continuous charge–discharge cycles. The strategy of preparation of a 3D macroscopic GMH is expected to realize promising high-performance hydrogel electrodes based on graphene and MXene for electrochemical energy storages.

© 2020 Author(s). All article content, except where otherwise noted, is licensed under a Creative Commons Attribution (CC BY) license (<http://creativecommons.org/licenses/by/4.0/>). <https://doi.org/10.1063/5.0015426>

I. INTRODUCTION

Supercapacitors (SCs), as an important member in various energy conversion and storage systems, have been useful in many challenging applications requiring enough power for a relatively short time or numerous rapid charge–discharge cycles.^{1–3} Much effort has been put on improving the energy density of SCs without sacrificing the power density or cycle stability.^{4,5} The high ion transport and electronic conductivity, together with the large specific surface area of electrode materials, form the vital factors to realize high electrochemical performance for SCs as they can facilitate the storage of more energy via the electric double layer or electrochemical reactions occurring at the electrode/electrolyte interface.⁶ With these in mind, research in electroactive materials

with three-dimensional (3D) hierarchical porous structures has attracted significant attention as the macropores afford ion accessibility to active surface while micro- and mesopores contribute to high specific surface area. 3D macroscopic hydrogels with cross-linked networks imbibing water and swelling are candidates for emerging electrode materials owing to their controllable hierarchical porous structures and attractive mechanical properties.^{7,8}

Graphene, a two-dimensional (2D) carbon material with a thickness of one single atom, has drawn great attention all over the world in the past decades due to its superior electrical conductivity, high specific surface area, and excellent mechanical properties.⁹ Self-assembling of 3D macroscopic graphene hydrogel can be achieved via a π – π stacking interaction of 2D graphene nanosheets

through a common “bottom-up” approach such as hydrothermal treatment¹⁰ or mild chemical reduction of graphene oxide (GO) with various reducing agents.¹¹ Among them, the hydrothermal process is more convenient, scalable, and environmentally friendly. The reduction of GO can lead to an improved conductivity which should be good for the charge transfer in SCs, hence resulting in enhanced electrochemical performance. In this case, it is reasonable to prepare graphene nanosheet-based hydrogels as electrode materials for SCs. However, the existence of a strong van der Waals interaction between adjacent graphene nanosheets often causes a large number of residual oxygen-containing groups and self-restacking graphene nanosheets, giving rise to a decrease in electronic conductivity, specific surface area, and electrochemical performance.^{10,11} Therefore, it is urgent to seek a type of material with high electronic conductivity for preventing the self-restacking of graphene nanosheets during the hydrothermal process.

Recently, a burgeoning family of nanosheets with graphene-like 2D morphology, transition metal nitrides and carbides (MXenes) with a general formula of $M_{n+1}X_nT_x$ (M, as early transition metal; X, carbon or nitrogen element; T, surface functional groups such as $-F$, $-O$, and $-OH$; and $n = 1, 2, 3$), have been studied as promising electrode materials for SCs owing to their high electrical conductivity and superior surface hydrophilicity.^{12–14} Such novel materials can be achieved by chemical etching out of the “A” element (mostly 13- or 14A-group) from the MAX phases with formula $M_{n+1}AX_n$.¹⁵ It is expected that MXene can serve as a functional additive to prevent the restacking of graphene nanosheets during the formation of graphene hydrogels and thus improve the electrochemical performance.

In this work, we report a facile one-step hydrothermal method for the preparation of a cylindrical-type 3D macroscopic graphene/MXene-based hydrogel (GMH) by self-assembling 2D laminar-structured GO and MXene (Ti_3C_2) nanosheets in Ar atmosphere and under the existence of ammonia water and hydrazine. The presence of ammonia water and hydrazine can make N-doped graphene with high reduction degree and palliate the oxidation of Ti_3C_2 to some extent, while the addition of Ti_3C_2 nanosheets can prevent the restacking of graphene nanosheets, leading to a large specific surface area and a high pore volume. The assembled symmetric SC based on GMH electrodes demonstrates a high energy density of 9.3 Wh kg^{-1} at a power density of 500 W kg^{-1} and an outstanding long-term cycle stability over 10 000 continuous charge–discharge cycles.

II. EXPERIMENTAL

A. Preparation of Ti_3C_2 suspension

The preparation of Ti_3C_2 suspension was carried out according to previous publications.^{16,17} Typically, 2 g of Ti_3AlC_2 powder (11 Technology Co., Ltd.) was added slowly into a 40 ml premixed solution of 2 g of LiF and 9M HCl, followed by continuous stirring at 35°C for 24 h. The resulting product was washed repeatedly with deionized water by centrifugations until the pH of the supernatant was ~ 6 . The sediment after centrifugation was re-dispersed in 300 ml of deionized water and sonicated in Ar atmosphere for 1 h, followed by centrifugation for 1 h at 3500 rpm. The obtained Ti_3C_2 suspension was collected for use.

B. Preparation of 3D macroscopic graphene/MXene hydrogel (GMH)

70 mg of GO powder (Nanjing XFNANO Materials Tech Co., Ltd.) was fully dispersed in 35 ml of 0.1 mg ml^{-1} Ti_3C_2 suspension with sonication in Ar atmosphere. Then, 70 μl of hydrazine hydrate and 490 μl of ammonia water were added to the mixture, which was sealed in a 50 ml autoclave vessel purged with Ar atmosphere, and maintained at 180°C for 6 h. The as-formed GMH was taken out with a pair of tweezers after the autoclave was cooled down to room temperature and washed repeatedly with deionized water to remove the residue. For comparison, a graphene hydrogel (GH) was also prepared via the hydrothermal process of 35 ml of 2 mg ml^{-1} GO aqueous dispersion at 180°C for 6 h without the addition of hydrazine hydrate and ammonia water.

C. Characterization

X-ray diffraction (XRD, Bruker D8 Advance X-ray) of the samples was performed using Cu K α radiation ($\lambda = 0.15406 \text{ nm}$) at 40 kV and 30 mA. The scanning speed was 5° min^{-1} with a 0.02° step. The morphology and structural properties of the samples were observed by scanning electron microscopy (SEM, LEO-1550) with an applied voltage of 5 kV and transmission electron microscopy (TEM, JEOL JEM-2010). X-ray photoelectron spectroscopy (XPS) was measured using a Thermo Scientific K-Alpha spectrometer. Raman spectra were obtained by using a Senterra Raman detection system (Bruker Optics) using a 532 nm laser beam. The nitrogen absorption/desorption isotherms were measured on the Micromeritics ASAP 2020 accelerated surface area and porosimetry system, and the surface area was calculated using the Brunauer–Emmett–Teller (BET) equation.

D. Electrochemical measurements

Two slices of the GMH were cut from the as-prepared cleaned hydrogel, placed on nickel foam, and compressed under a pressure of 15 MPa for 1 min, followed by soaking in a 6M KOH electrolyte for 1 h to exchange the water with the electrolyte. Then, the symmetric SC was assembled in a CR2016 coin cell using the two slices of the pre-treated GMH on nickel foam as electrodes and a filter paper as the separator. The electrochemical measurements were carried out at room temperature on a CHI660D electrochemical working station instrument. Cyclic voltammetry (CV) tests were performed at different scan rates, and galvanostatic charge/discharge (GCD) curves were measured at various current densities. Electrochemical impedance spectroscopy (EIS) was performed in the frequency range of 100 kHz–0.01 Hz at open-circuit potential with an AC perturbation of 5 mV. The specific capacitance (C , F g^{-1}), gravimetric energy density (E_g , Wh kg^{-1}), power density (P_g , W kg^{-1}), volumetric energy density (E_v , Wh l^{-1}), and power density (P_v , W l^{-1}) can be calculated based on the following equations:

$$C = \frac{I\Delta t}{m\Delta V}, \quad (1)$$

$$E_g = \frac{1}{7.2} C\Delta V^2, \quad (2)$$

$$P_g = 3600 \frac{E_g}{\Delta t}, \quad (3)$$

$$E_v = \rho E_g, \quad (4)$$

$$P_v = \rho P_g, \quad (5)$$

where I is the discharge current (A), Δt is the discharge time (s), ΔV is the potential window (V), m is the total mass of electrode materials (g), and ρ is the density of the GMH (g cm^{-3}).

III. RESULTS AND DISCUSSION

Figure 1(a) illustrates the preparation procedure of the GMH in the one-step hydrothermal process. GO powder was thoroughly dispersed in fresh Ti_3C_2 suspension (0.1 mg ml^{-1}), which was prepared in advance by etching of the MAX (Ti_3AlC_2) phase with LiF/HCl solution followed by delamination via sonication to obtain a mixture. After adding a certain amount of ammonia water and hydrazine, the mixture was sealed in an autoclave vessel at 180°C for 6 h. The whole process was carried out in Ar atmosphere. After complete reaction, a 3D macroscopic GMH with a height of $\sim 2.5 \text{ cm}$ and a diameter of $\sim 1.2 \text{ cm}$ has been formed due to the π - π stacking interaction of nanosheets [Fig. 1(b)]. However, no hydrogel forms when using single Ti_3C_2 or GO nanosheets as a raw material under identical conditions (Fig. S1), which could be due to the insufficient interactions between the nanosheets and the ineffective trap of water into nanosheets after hydrothermal treatment.¹⁸ For comparison, a graphene hydrogel (GH) based on self-assembling of pure GO dispersion (2 mg ml^{-1}) was prepared in the absence of ammonia water and hydrazine [Fig. 1(b)]. The size of the GH (a height of $\sim 2 \text{ cm}$ and a diameter of $\sim 1 \text{ cm}$) is little smaller than that of the GMH, indicating that Ti_3C_2 can prevent the self-restacking of graphene nanosheets to some extent during the hydrothermal process.

The structure and morphologies of the materials were investigated by SEM. A large corrugated laminar morphology and a layered accordion-like structure can be observed in GO (Fig. S2a) and Ti_3C_2 (Fig. S2b in the supplementary material), respectively.¹⁹ As shown in Figs. 2(a) and 2(b), the GMH features a well-defined and interconnected 3D porous network with random open pores and thin pore walls. The interconnected network structure with thin nanosheets can also be verified by TEM, as displayed in Fig. 2(c). In addition, the HRTEM of the GMH showed a lattice spacing of 0.354 nm , which was corresponding to the (101) crystal planes of TiO_2 , indicating the oxidation of Ti_3C_2 to some extent during the hydrothermal treatment. Similar to that of the GMH, the GH also exhibits a 3D porous structure which looks much denser than that of the GMH (Fig. S3). To further examine the porous structure, Fig. 2(d) shows the nitrogen adsorption-desorption isotherm with a H2 type hysteresis loop for both hydrogels. The BET surface area and pore volume of the GMH are measured to be $161.1 \text{ m}^2 \text{ g}^{-1}$ and $0.5 \text{ cm}^3 \text{ g}^{-1}$, respectively, which are ~ 4 times larger than those of the GH ($33.6 \text{ m}^2 \text{ g}^{-1}$ and $0.1 \text{ cm}^3 \text{ g}^{-1}$, respectively), confirming the highly interconnected porous network caused by the mitigative restacking laminar structure of graphene nanosheets. The micropore area and external surface area of the GMH are $13.0 \text{ m}^2 \text{ g}^{-1}$ and $148.1 \text{ m}^2 \text{ g}^{-1}$, respectively. In addition, a well-distinguished maximum can be observed centered at $\sim 2.4 \text{ nm}$ in the pore size distribution plot of the GMH (Fig. S4). The improved porous structure is quite benefit for the electrolyte ion transport during the electrochemical process.

The crystallographic structures of various samples were investigated by XRD, as shown in Fig. 3. After etching Al from the Ti_3AlC_2 phase, the obtained Ti_3C_2 exhibits characteristic (001) peaks with an interlayer spacing of 1.41 nm calculated from the (002) peak at 6.25° . For the GH, the diffraction peak at around 25.7° (002) is corresponding to an interlayer spacing of 0.35 nm which is much lower than that of the raw material GO (0.875 nm),²⁰ suggesting the

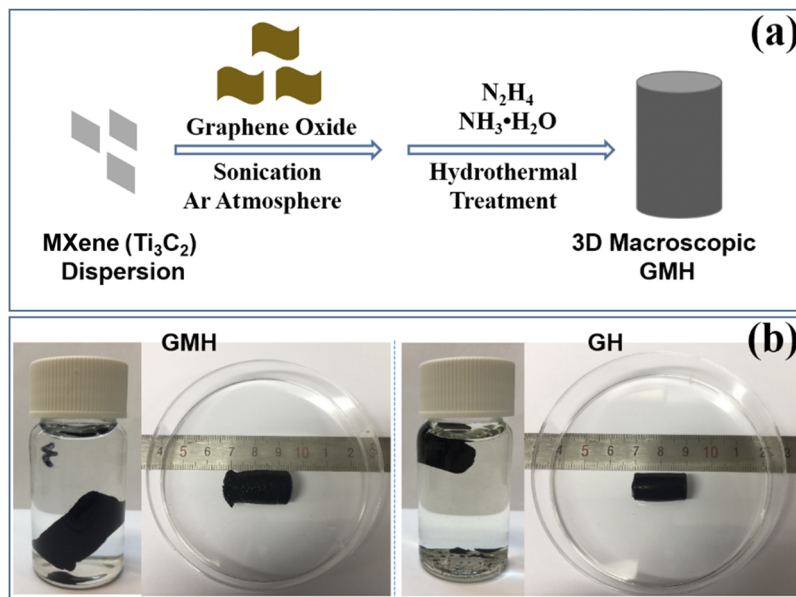


FIG. 1. (a) Preparation procedure of the GMH. (b) Digital photos of the GMH and GH.

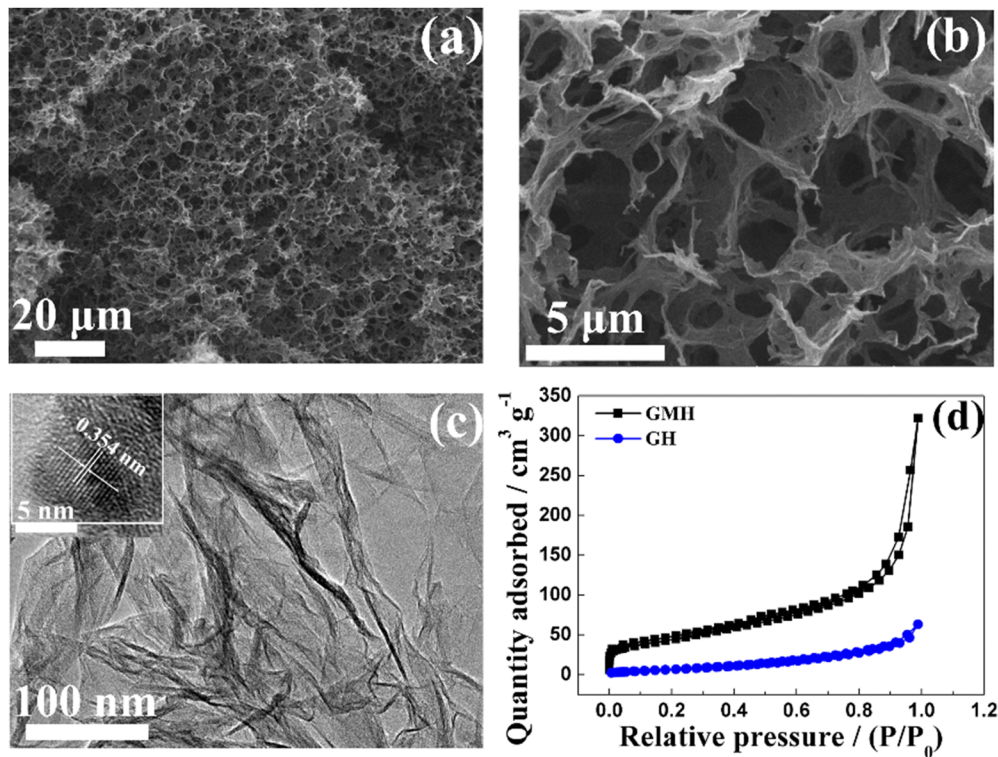


FIG. 2. (a) and (b) SEM images and (c) TEM image of the GMH (inset: HRTEM of the GMH). (d) N_2 adsorption–desorption isotherms of the GMH and GH.

reduction reaction of GO during the hydrothermal process, while for the GMH, only the diffraction peak of graphene at around 25° was detected, which is similar to that of the GH. Other crystalline phases such as Ti_3C_2 and TiO_2 cannot be detected, which could be due to the low amount in the GMH. The phenomenon has also been observed in other published papers.^{14,21} However, in contrast, when graphene/MXene mixture solution reacted in the conventional

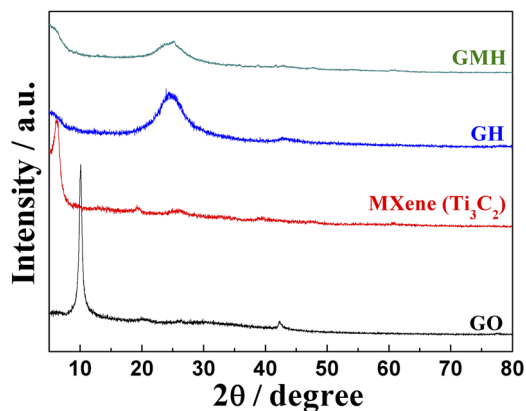


FIG. 3. XRD patterns of samples: GO, MXene (Ti_3C_2), GH, and GMH.

hydrothermal process without the addition of ammonia water and hydrazine, the XRD pattern of the as-obtained material showed the existence of TiO_2 (JCPDS No. 21-1272) (Fig. S5), confirming the palliative oxidation of Ti_3C_2 in our proposed method.²²

Figure 4(a) shows the Raman spectra of the as-obtained materials. For Ti_3C_2 , the peaks are assigned to the out-of-plane (198 cm^{-1}) and in-plane (282 cm^{-1} , 394 cm^{-1} , and 622 cm^{-1}) modes of Ti, C, and the terminal group atoms.¹⁷ For other three materials, two characteristic peaks at around 1350 cm^{-1} and 1600 cm^{-1} can be found in both samples, corresponding to the D (a breathing mode of k -point photons of the A_{1g} symmetry) and G bands (the first-order scattering of the E_{1g} phonon of sp^2 C atoms) of the carbon material, respectively. The peak intensity ratio of the D and G bands, I_D/I_G , is a useful indicator to evaluate the disorder degree and average size of the sp^2 domains of the graphite materials. Based on the spectra, the I_D/I_G value can be calculated to be 1.08 for the GMH, which is higher than that of the GH (0.98) and GO (0.88), indicating the formation of more structural defects as well as the reduction of GO after the hydrothermal process.

XPS was performed to examine the chemical composition and the surface electronic state of the materials. The C 1s XPS spectra of the GH exhibit much weaker intensities of oxygenated functionalities (Fig. S6), C–O (286.4 eV) and C=O (288.0 eV), than those of GO, and the C/O atomic ratio increases from 2.05 of GO to 5.54 of the GH, also confirming the reduction of GO after the hydrothermal process. In Fig. 4(b), the XPS survey spectrum of Ti_3C_2 shows

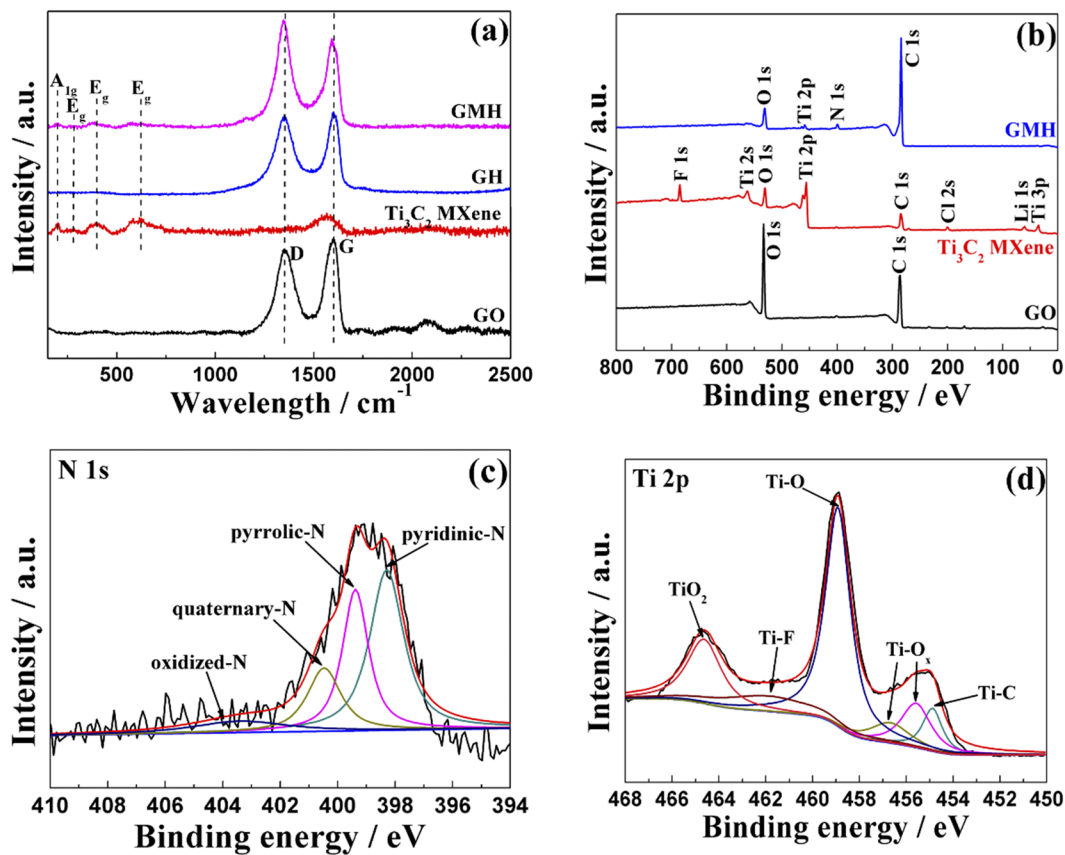


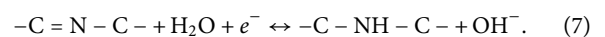
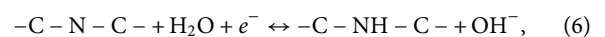
FIG. 4. (a) Raman spectra of samples: GO, Ti₃C₂, GH, and GMH. (b) XPS survey spectra of the GMH and Ti₃C₂; high-resolution XPS spectra of the GMH: (c) N 1s and (d) Ti 2p.

the characteristic signals of Cl 1s, C 1s, Ti 2p, O 1s, F 1s, and so on.²³ In contrast, it can be obviously observed that no F 1s signal is detected and an additional signal of N 1s appears at ~400 eV in the GMH. The detected N atom is due to the addition of ammonia water and hydrazine, with three well-fitted peaks centered at 398.3 eV, 399.4 eV, 400.4 eV, and 403.4 eV corresponding to the pyridinic N, pyrrolic N, graphitic N, and oxidized N, respectively [Fig. 4(c)].²⁰ The N-doped carbon materials are reported to benefit charge transfer and thus improve the electrochemical performance of carbon materials. The Ti 2p peaks of the GMH are assigned to Ti–C, Ti–O_x, Ti–O, and TiO₂, respectively [Fig. 4(d)].²² In addition, the C 1s peaks of the GMH belong to Ti–C, C–C, C–O/C–F, and C=O, respectively (Fig. S6c), which also confirm the reduction of GO and existence of Ti₃C₂ in the GMH.

Based on the aforementioned characteristic results, the formation mechanism of the GMH can be proposed as follows: GO can be reduced to graphene sheets under the hydrothermal condition. With the reaction proceeding, the hydrophobicity and π - π interactions of graphene sheets would generate enough cross-linking sites to form a 3D porous network; meanwhile, the residual oxygen-containing functional groups could entrap water into the 3D network.¹⁰ In addition, Ti₃C₂ would be incorporated into the porous network via the

van der Waals forces and hydrogen bonding between Ti₃C₂ and graphene.¹⁷ During the process, the ammonia water and hydrazine not only made graphene sheets doped with nitrogen species but also eliminated the amount of functional groups (hydroxyl and fluoride) and palliated the oxidation of Ti₃C₂ to some extent.²⁴ Finally, a GMH with 3D porous network was successfully prepared.

To investigate the feasibility of the as-obtained GMH as electrodes in practical applications for SCs, two pieces of GMH slices cut from the 3D macroscopic GMH were used directly as electrodes for assembling a symmetric SC in a 6M KOH aqueous electrolyte without any binders or conducting additives. It is obvious that the CV curves exhibit nearly rectangular shape under the scan rates from 5 mV s⁻¹ to 100 mV s⁻¹, indicating an ideal capacitive behavior and fast charging/discharging kinetics [Fig. 5(a)]. However, compared with the complete rectangular shape, the CV curves exhibited a certain deviation due to a certain amount of functional groups on the surface. The corresponding reactions could occur as follows:²⁵



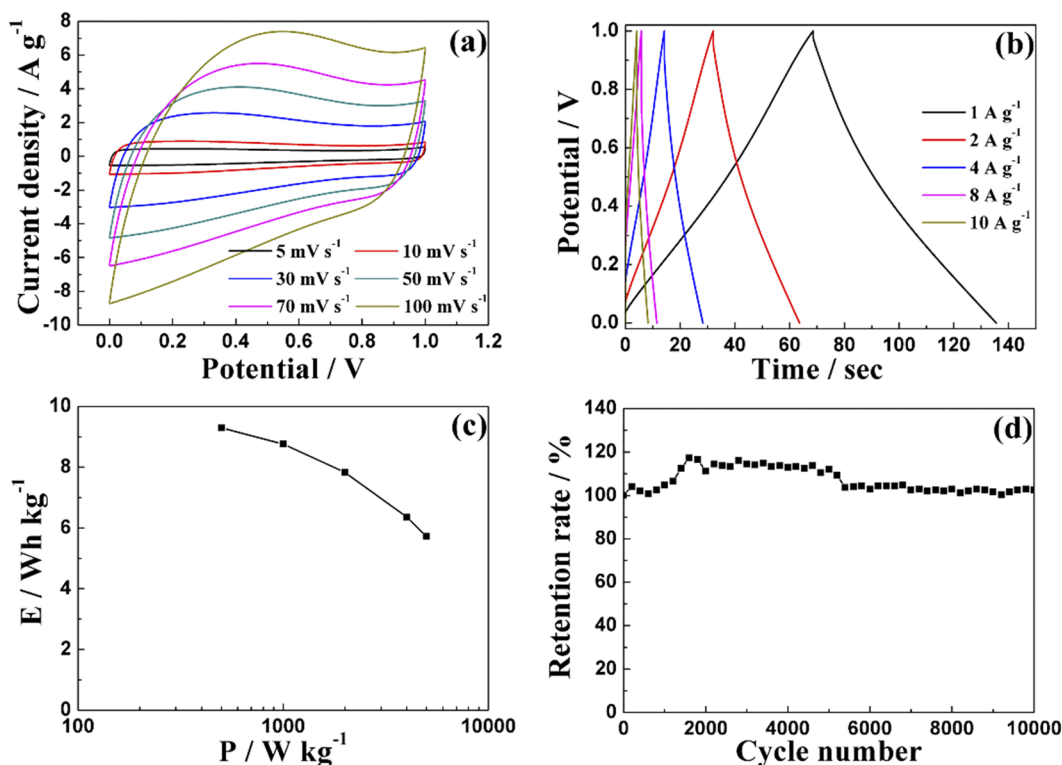


FIG. 5. (a) CV curves of the GMH-based SC at different scan rates; (b) GCD curves of the GMH-based SC at various current densities; (c) the Ragone plot of the GMH-based SC; (d) cycle stability of the GMH-based SC at 4 A g^{-1} .

The GCD profiles and the calculated capacitance of SCs are depicted in Fig. 5(b) and Fig. S7, respectively. All of the GCD curves are ideal symmetric, illuminating the high reversibility, which is consistent with the CV results. In addition, the EIS data of the GMH showed lower internal resistance (the intercept of the curve with the real axis in the high-frequency region), charge transfer resistance (the diameter of the semicircle in the medium-frequency region), and a larger slope of the straight line in the low-frequency region (Fig. S8), confirming the enhanced conductivity and improved porous structure for efficient charge transfer and ion transportation.²⁶ The calculated specific capacitance of the GMH electrode can reach to 267.7 F g^{-1} and 164.8 F g^{-1} at a current density of 1 A g^{-1} and 10 A g^{-1} , respectively. Figure 5(c) exhibits the Ragone plot of the as-assembled SC. The device displays a high gravimetric energy density of 9.3 Wh kg^{-1} at a power density of 500 W kg^{-1} . Even at a higher power density of 5000 W kg^{-1} , the device still possesses a gravimetric energy density of 5.7 Wh kg^{-1} . The results show that our SC device based on GMH electrodes achieved higher energy density than the reported devices. Accordingly, the volumetric energy density reaches up to 13.1 Wh l^{-1} at a volumetric power density of 706.5 W l^{-1} and retains 8.1 Wh l^{-1} at an excellent volumetric power density of 7065 W l^{-1} (Fig. S9). Moreover, as shown in Fig. 5(d), the device exhibits excellent cycle stability with no loss in capacitance over 10 000 continuous charge–discharge cycles at a current density of 4 A g^{-1} , which could be due to the high structural

stability and strong interaction between the nanosheets (Fig. S10). The enhanced capacitance during the initial 2000 cycles can be attributed to the improvement of ion accessibility in 3D frameworks during the cycling process, which leads to an increased accommodation behavior for charges.²⁷ The remarkably outstanding electrochemical performance can be attributed to two reasons: first, the interconnected 3D porous network with random open pores and thin pore walls due to the mitigative restacking laminar structure of graphene nanosheets is quite benefit for the fast adsorption and diffusion of electrolyte ions on the electrode surface; second, the N atoms generated from ammonia water and hydrazine are doped onto graphene, which supply additional negative charges facilitating the charge transfer and thus improve the electrochemical performance.

IV. CONCLUSION

In summary, we have developed a facile strategy for the synthesis of a high performance energetically stable 3D macroscopic GMH. The GMH could prevent self-restacking of the laminar structure, forming an interconnected 3D porous network structure, and N atoms are doped onto the GMH, facilitating the charge transfer in the electrode. Benefiting from the unique configuration, a symmetric SC assembled by GMH slices displays superior electrochemical performance such as high capacitance and energy density and outstanding long-term cycle stability. It is expected that the work presented

here can present a new way to create graphene/Mxene electrodes for energy storage devices.

SUPPLEMENTARY MATERIAL

See the [supplementary material](#) for digital photos of samples prepared by pure Ti_3C_2 or GO under the existence of ammonia water and hydrazine hydrate; SEM images of GO and Ti_3C_2 ; SEM and TEM images of the GH; pore size distribution plots of the GH and GMH; XRD patterns of samples prepared by the hydrothermal treatment of graphene/MXene mixture solution without the addition of ammonia water and hydrazine; high-resolution C 1s XPS spectra of GO, GH, and GMH; specific capacitance of the GMH electrode in the GMH-based SC at various current densities; EIS measurements of GMH and GH-based SCs. Volumetric energy and power densities of GMH-based SCs. SEM image of the GMH after the cycling test.

ACKNOWLEDGMENTS

This work was supported by the Research Grants Council of the HKSAR Government (Grant Nos. 15217917 and R5020-18), The Hong Kong Polytechnic University (Grant No. 1-YW3C), and the Innovation and Technology Commission of the HKSAR Government to the Hong Kong Branch of National Rail Transit Electrification and Automation Engineering Technology Research Center (Grant No. K-BBY1).

DATA AVAILABILITY

The data that support the findings of this study are available from the corresponding author upon reasonable request.

REFERENCES

- ¹K. S. Kumar, N. Choudhary, Y. Jung, and J. Thomas, *ACS Energy Lett.* **3**, 482 (2018).
- ²M. Zhang, L. He, T. Shi, and R. Zha, *Chem. Mater.* **30**, 7391 (2018).
- ³R. R. Salunkhe, Y. V. Kaneti, and Y. Yamauchi, *ACS Nano* **11**, 5293 (2017).
- ⁴H. Pan, D. Wang, Q. Peng, J. Ma, X. Meng, Y. Zhang, Y. Ma, S. Zhu, and D. Zhang, *ACS Appl. Mater. Interfaces* **10**, 10157 (2018).
- ⁵X. Wang, A. Y. Mehandziyski, B. Arstad, K. L. Van Aken, T. S. Mathis, A. Gallegos, Z. Tian, D. Ren, E. Sheridan, B. A. Grimes, D.-e. Jiang, J. Wu, Y. Gogotsi, and D. Chen, *J. Am. Chem. Soc.* **139**, 18681 (2017).
- ⁶Y. Shao, M. F. El-Kady, J. Sun, Y. Li, Q. Zhang, M. Zhu, H. Wang, B. Dunn, and R. B. Kaner, *Chem. Rev.* **118**, 9233 (2018).
- ⁷J. Mao, J. Iocozzia, J. Huang, K. Meng, Y. Lai, and Z. Lin, *Energy Environ. Sci.* **11**, 772 (2018).
- ⁸Y. Guo, J. Bae, F. Zhao, and G. Yu, *Trends Chem.* **1**, 335 (2019).
- ⁹C. Lu, J. Meng, J. Zhang, X. Chen, M. Du, Y. Chen, C. Hou, J. Wang, A. Ju, X. Wang, Y. Qiu, S. Wang, and K. Zhang, *ACS Appl. Mater. Interfaces* **11**, 25205 (2019).
- ¹⁰Y. Xu, K. Sheng, C. Li, and G. Shi, *ACS Nano* **4**, 4324 (2010).
- ¹¹W. Chen and L. Yan, *Nanoscale* **3**, 3132 (2011).
- ¹²M. R. Lukatskaya, O. Mashtalir, C. E. Ren, Y. Dall'Agnese, P. Rozier, P. L. Taberna, M. Naguib, P. Simon, M. W. Barsoum, and Y. Gogotsi, *Science* **341**, 1502 (2013).
- ¹³M. Ghidui, M. R. Lukatskaya, M.-Q. Zhao, Y. Gogotsi, and M. W. Barsoum, *Nature* **516**, 78 (2014).
- ¹⁴Y. Yue, N. Liu, Y. Ma, S. Wang, W. Liu, C. Luo, H. Zhang, F. Cheng, J. Rao, X. Hu, J. Su, and Y. Gao, *ACS Nano* **12**, 4224 (2018).
- ¹⁵R. Li, L. Zhang, L. Shi, and P. Wang, *ACS Nano* **11**, 3752 (2017).
- ¹⁶J. Yan, C. E. Ren, K. Maleski, C. B. Hatter, B. Anasori, P. Urbankowski, A. Sarycheva, and Y. Gogotsi, *Adv. Funct. Mater.* **27**, 1701264 (2017).
- ¹⁷Z. Fan, Y. Wang, Z. Xie, D. Wang, Y. Yuan, H. Kang, B. Su, Z. Cheng, and Y. Liu, *Adv. Sci.* **5**, 1800750 (2018).
- ¹⁸D. Long, W. Li, L. Ling, J. Miyawaki, I. Mochida, and S.-H. Yoon, *Langmuir* **26**, 16096 (2010).
- ¹⁹S. Xu, G. Wei, J. Li, W. Han, and Y. Gogotsi, *J. Mater. Chem. A* **5**, 17442 (2017).
- ²⁰H. H. Shi, S. Jang, A. Reza-Ugalde, and H. E. Naguib, *ACS Appl. Energy Mater.* **3**, 987 (2020).
- ²¹Y. Chen, X. Xie, X. Xin, Z.-R. Tang, and Y.-J. Xu, *ACS Nano* **13**, 295 (2019).
- ²²G. Jia, Y. Wang, X. Cui, and W. Zheng, *ACS Sustainable Chem. Eng.* **6**, 13480 (2018).
- ²³L. Li, M. Zhang, X. Zhang, and Z. Zhang, *J. Power Sources* **364**, 234 (2017).
- ²⁴O. Mashtalir, M. R. Lukatskaya, A. I. Kolesnikov, E. Raymundo-Piñero, M. Naguib, M. W. Barsoum, and Y. Gogotsi, *Nanoscale* **8**, 9128 (2016).
- ²⁵W. J. Zhang, Z. T. Chen, X. L. Guo, K. Jin, Y. X. Wang, L. Li, Y. Zhang, Z. M. Wang, L. T. Sun, and T. Zhang, *Electrochim. Acta* **278**, 51 (2018).
- ²⁶L. J. Zhang, K. N. Hui, K. S. Hui, and S. W. Or, *Dalton Trans.* **48**, 150 (2019).
- ²⁷Z.-S. Wu, Y. Sun, Y.-Z. Tan, S. Yang, X. Feng, and K. Müllen, *J. Am. Chem. Soc.* **134**, 19532 (2012).